Available online at www.sciencedirect.com
ScienceDirect
Journal of Power Sources 173 (2007) 233–239
JOURNAL OF POWER SOURCES
www.elsevier.com/locate/jpowsour

Computational analysis of thermo-fluid and electrochemical characteristics of MOLB-type SOFC stacks

Yunzhen Yang [a,*], Guilan Wang [a], Haiou Zhang [b], Weisheng Xia [a]

[a] State Key Laboratory of Material Processing and Die & Mould Tech., Huazhong University of Sci. & Tech., Wuhan 430074, PR China
[b] State Key Laboratory of Digital Manufacturing and Equipment Tech., Huazhong University of Sci. & Tech., Wuhan 430074, PR China

Received 15 April 2007; received in revised form 5 June 2007; accepted 15 June 2007
Available online 23 June 2007

Abstract

A 3D simulation tool for solid oxide fuel cells (SOFCs) was described to simulate the mass, momentum and energy conversions in the monoblock layers built (MOLB)-type SOFC system. Considering the co-flow and counter-flow cell designs, the temperature distributions, variations of reaction species and current densities of the single-unit cell were calculated under the different working conditions. The simulation results show that the co-flow case has more uniform temperature and current density distributions. Similar to the planar SOFC, in co-flow case, increasing fuel delivery rate or hydrogen mass fraction in the fuel, average temperatures of PEN (positive/electrolyte/negative) and current densities rise, but the average temperatures of PEN decrease with increasing the delivery rate of air. In particular, MOLB-type SOFC has some advantages such as: higher hydrogen utilizations, lower temperature difference and higher current density. However the current density distributions are less uniform in MOLB-type SOFC, which is a disadvantage in this type SOFC.

Keywords: MOLB-type SOFC; Thermo-fluid model; Electrochemical model; Temperature distribution; Current density

1. Introduction

The solid oxide fuel cell (SOFC) is expected to be a promising alternative power source for distributed or residential power plants because of its higher energy conversion efficiency and power density, lower environmental hazards and production cost [1–3]. However, the further development of SOFC stacks faces the challenges related to maximize the power density and to minimize the non-uniform temperature distribution, which contributes to the thermal stress in the SOFC components [4,5].

At this stage of SOFC stack development, design of geometry is almost as crucial as material development. In the past, some focus has been placed on the designs of new material [6–9] or novel geometry [10–13]. Besides planar and tubular SOFCs, recently, MOLB-type SOFC also has been drawn keen attention and researched to improve the comprehensive performance of SOFC. In the MOLB-type SOFC, the corrugated-shaped PEN not only ensures the effective electrochemical reaction area is higher than the projected area, but also provides the film with the combined function of fuel and airflow paths, making the cell compact and saving the laborious work of channel machining.

In addition to the geometrical designs of SOFC, the working conditions, such as delivery rate of gas to the cell system (including the fuel and air gas), and hydrogen mass fraction in fuel gas also influence the performances of SOFC in a complicated way. Therefore, it is difficult and uneconomical to investigate the influences of these parameters independently by testing methods. The computer simulation technique has been used to analyze effectively the process of energy conversion in the SOFC system. Some modeling of the SOFC during steady operation has been constructed to calculate temperature and current density distributions [14–20]. Investigations of planar and MOLB-type SOFC operation and performance have predicted cell temperature and current density distributions for various flow patterns [21–24]. However, only a little work has been performed on the influences of the operating conditions on the performances of planar SOFC [25,26], or even saying nothing of the MOLB-type SOFC.

* Corresponding author. Tel.: +86 27 62475231.
E-mail address: yyzhenhust@hotmail.com (Y. Yang).

0378-7753/$ – see front matter © 2007 Published by Elsevier B.V.
doi:10.1016/j.jpowsour.2007.06.070

Nomenclature

C_p	specific heat (J kg^{-1} K^{-1})
C_k	concentration of component k
$D_{k,eff}$	effect diffusivity of component k (m^2 s^{-1})
E_f	internal energy of mixture gas (J)
E_s	internal energy of solid (J)
F	Faraday constant (C mol^{-1})
i	local current density (A cm^{-2})
I_k	mass source of mixture component k
j	transfer current density (A cm^2)
k_{eff}	effect thermal conductivity coefficient (W m^{-1})
k_f	thermal conductivity coefficient of gas (W m^{-1})
k_s	thermal conductivity coefficient of solid (W m^{-1})
K	permeability coefficient (m^2)
P	pressure of mixture (Pa)
R	gas constant (J mol^{-1} K^{-1})
s_k	reaction coefficient of component k
S_E	energy source (J)
S_M	momentum source
ΔS	entropy change (J mol^{-1})
T	temperature (K)
U	mixture velocity (m s^{-1})

Greek letters

ε	porosity
δ	anode thickness (m)
$\eta_{act,a}$	activation potential at anode (V)
$\eta_{act,c}$	activation potential at cathode (V)
μ_{eff}	effect viscosity
ρ	density (kg m^{-3})
σ_{eff}	effect electrical conductivity (Ω^{-1} m^{-1})

The objective of present work is to simulate the thermal and electrochemical performances of MOLB-type SOFC. A computational fluid dynamics (CFD) model tool is demonstrated to predict temperature, species mass fraction and current density distributions in SOFC system. The results simulated in this paper can not only guide the designer in understanding how geometrical design affects thermodynamics performances and electrochemical characteristics of the SOFC, but also provide a more reasonable basis for designing geometry and choosing working conditions of the SOFC stacks.

2. Model development

2.1. Geometry of MOLB-type SOFC

As shown in Fig. 1, a typical MOLB-type SOFC [13] is symmetric about the mid-planes of the air and fuel channels. For the sake of simplicity in the simulation, the calculation domain includes the region between these two mid-planes [21]. The thicknesses of anode, cathode, electrolyte and inter-connector were 0.5, 0.25, 0.05 and 1.0 mm, respectively.

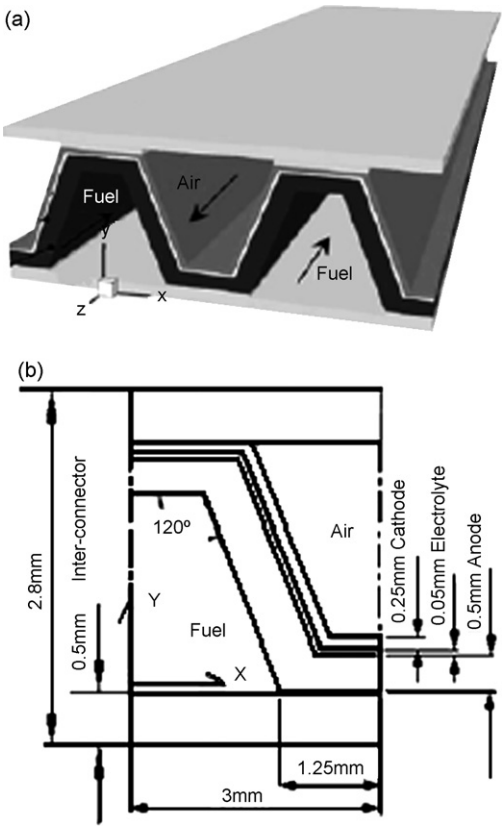

Fig. 1. Illustrations of the one cell-stack and the single unit model for MOLB-type SOFC.

2.2. Thermo-fluid model

In the simulation, the solid and fluid domains were divided into some discrete meshes, and in each computational mesh, the conservation equations of species, mass, momentum and energy were solved using the finite volume method.

The species conservation equation:

$$\nabla(\rho C_k U) = \nabla(D_{k,\text{eff}}\nabla C_k) + I_k, \quad k = \text{H}_2, \text{O}_2, \text{H}_2\text{O} \tag{1}$$

where I_k is the rate of production or the consumption of specie k, and given by [27]:

$$I_k = \pm\frac{(s_k j)}{(2F)} \tag{2}$$

The diffusion coefficients of hydrogen and oxygen are obtained as follow [27]:

$$D_{\text{O}_2} = 0.181\left(\frac{T}{273}\right)^{1.5}, \quad D_{\text{H}_2} = 0.753\left(\frac{T}{273}\right)^{1.5} \tag{3}$$

The mass conservation equation:

$$\nabla \cdot (\varepsilon\rho U) = 0 \tag{4}$$

The gas was considered as ideal gas mixtures with the densities given by:

$$\rho = \frac{P}{RT}\left(\sum_k \left(\frac{m_k}{M_k}\right)\right) \tag{5}$$

where m_k is the mass fraction of specie k with molecular weight M_k.

The momentum conservation equation:

$$\rho\varepsilon\left(u\frac{\partial u}{\partial x}+v\frac{\partial v}{\partial y}+w\frac{\partial w}{\partial z}\right) = -\varepsilon\nabla P+\varepsilon\mu_{\text{eff}}\left(\frac{\partial u^2}{\partial x^2}+\frac{\partial v^2}{\partial y^2}+\frac{\partial w^2}{\partial z^2}\right)+S_{\text{M}} \quad (6)$$

where S_{M} is momentum source, and $S_{\text{M}}=0$ in the flow channels. However, in the porous electrodes, Darcy law with constant porosity and permeability is applied to the model and the momentum source is obtained by [27]:

$$S_{\text{M}}=-\left(\frac{\mu_{\text{eff}}}{K}\right)\varepsilon^2 U \quad (7)$$

where u_{eff} is the effective viscosity of the mixture gas and is given by [27]:

$$\mu_{\text{eff}}=\sum_k\left(\frac{X_k\mu_k}{\sum_k X_k\phi_{kj}}\right) \quad (8)$$

$$\phi_{kl}=\left(\frac{[1+(\mu_k/\mu_j)^{1/2}(M_j/M_k)^{1/4}]^2}{\left[8(1+(M_k/M_j))\right]^{1/2}}\right) \quad (9)$$

where X_k is the molar percent of the specie k, μ_j and μ_k are kinematical viscosities of specie j and k, respectively.

The energy conservation equation:

$$\nabla\cdot(U(\rho_{\text{f}}E_{\text{f}}+p))+\nabla\cdot(\tau U)+\nabla\cdot(k_{\text{eff}}\nabla T)+S_{\text{E}}=0 \quad (10)$$

Heat transfer between the fluid and the solid materials was limited to conduction and convection, and the effect of radiation was neglected in this calculation because it is very small relative to the other kinds of heat transfer. Additionally, the effective thermal conductivities of porous electrodes are calculated by the Eq. (11) [28]:

$$k_{\text{eff}}=\varepsilon k_{\text{f}}+(1-\varepsilon)k_{\text{s}} \quad (11)$$

where k_{f} and k_{s} are thermal conductivities of fluid and solid, respectively. S_{E} is the energy source expressed by the Eq. (12) and mainly consists of reaction and Ohmic heats [27].

$$S_{\text{E}}=\frac{i^2}{\sigma_{\text{eff}}}+\left(\frac{i}{\delta}\right)\left(\left(\frac{T\Delta S}{2F}\right)+\eta_{\text{act}}\right) \quad (12)$$

Specific heats of gas components are described as the functions of temperature [27]:

$$C_{\text{p}}=a+b\times10^3T+c\times10^6T^2 \quad (13)$$

Table 1
Coefficients of the specific heats of gas

Gas	a	b	c
Hydrogen	25.8911	−0.8373	2.0138
Oxygen	29.0856	12.9874	−3.8644
Water gas	30.3794	9.6212	1.1848

where a, b and c are relevant coefficients, as listed in Table 1. Solid material properties used in this simulation are listed in Table 2.

2.3. Electrochemical model

The oxidant reduction reaction occurring at the cathode is expressed as follows:

$$0.5O_2+2e^-\rightarrow O^{2-} \quad (14)$$

The oxygen ions transfer through the electrolyte and then into the active reaction areas of anode. The electrochemical reaction of fuel at the anode is:

$$H_2+O^{2-}\rightarrow H_2O+2e^- \quad (15)$$

So the overall reaction is:

$$H_2+0.5O_2\rightarrow H_2O \quad (16)$$

According to the Faraday law, the reaction rates depend on the current density i [15]:

$$i=2F\frac{\text{d}f}{\text{d}t}=4F\frac{\text{d}O_2}{\text{d}t} \quad (17)$$

where $\text{d}f/\text{d}t$, $\text{d}O_2/\text{d}t$ are the molar consumption rates of fuel and oxygen at the anode and the cathode, respectively.

During the process of energy conversion, when the charge transfer reactions at the interfaces of electrolyte and electrode are too slow to provide ions at the rate required by the demands of current, the activation polarization occurs and is defined by the Butler–Volmer equation [28]:

$$i=i_0\left\{\exp\left(-\beta\left(\frac{2F}{RT}\right)\eta_{\text{act}}\right)-\left[\exp(1-\beta)\left(\frac{2F}{RT}\right)\eta_{\text{act}}\right]\right\} \quad (18)$$

Eq. (18) is simplified and described by the Tafel empirical formula [28,29]:

$$\eta_{\text{act,a}}=\left(\frac{RT}{2Fi_{0\text{a}}}\right)i \quad (19)$$

Table 2
Properties of the solid material

Cell component	Density (kg m^{-3})	Effect thermal conductivity (W m^{-1} K^{-1})	Specific heat (J kg^{-1} K^{-1})	Porosity (%)	Permeability coefficient (m^2)
Inter-connector	7700	13	0.8	–	–
Anode	6200	6.23	0.65	35	1.0E−12
Cathode	6000	9.6	0.9	35	1.0E−12
Electrolyte	5560	2.7	0.3	–	–

$$\eta_{\mathrm{act,c}} = -\left(\frac{RT}{2\beta F}\right)\ln i_{0\mathrm{c}} + \left(\frac{RT}{2\beta F}\right)\ln i \tag{20}$$

where β is the transmission coefficient and $\beta = 0.5$ in this simulation, $\eta_{\mathrm{act,a}}$ and $\eta_{\mathrm{act,c}}$ are the activation potentials at the anode and the cathode, respectively. $i_{0,\mathrm{a}}$ and $i_{0,\mathrm{c}}$ are the exchange current densities at the anode and the cathode, respectively.

A simple semi-empirical formula is used to obtained the Nernst voltage:

$$E = E_0 + \frac{RT}{(2F)}\ln\left(\frac{p_{\mathrm{H_2O}}}{p_{\mathrm{H_2}}\,p_{\mathrm{O_2}}^{0.5}}\right) = \frac{RT}{(2F)}\ln K + RT\ln\left(\frac{p_{\mathrm{H_2}}\,p_{\mathrm{O_2}}^{0.5}}{p_{\mathrm{H_2O}}}\right) \tag{21}$$

where E_0 is the standard voltage of the cell, $P_{\mathrm{H_2O}}$, $P_{\mathrm{O_2}}$ and $P_{\mathrm{H_2}}$ are the partial pressures of water gas, oxygen and hydrogen, respectively.

3. Numerical implementation

The cell unit analyzed in the paper represented a repeating unit in the middle of a large stack, and external walls of the cell unit were assumed to be adiabatic. Constant temperature, delivery rate, and gaseous composition were imposed at the inlet boundaries for the fuel and air.

In the calculations, the modeling tool coupled a thermal-fluid model with an electrochemical model. The thermal-fluid model was implemented via the commercial CFD simulation code. First, the finite-volume Navier-Stokes and transport equations were solved to obtain the gas species concentrations and temperatures at each position in the cell. Then, the information was passed to the electrochemical model, which was called via the subroutine. Using this solution, the Nernst voltage and the current density distribution were calculated and applied to obtain heat source and species source. Finally, gas species concentrations and temperature distributions were then calculated again and provide for the next iteration. The models were coupled time after time until convergence of solution was achieved.

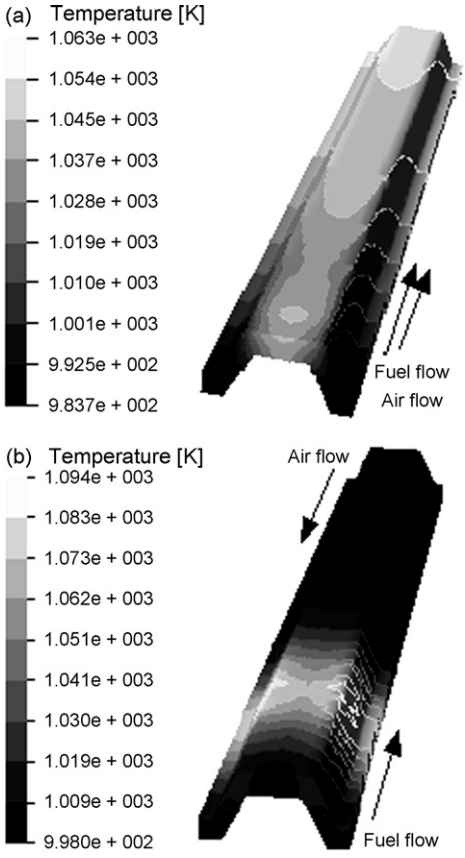

Fig. 2. PEN temperature distributions in the co-flow case (a) and counter-flow case and (b) under first working conditions.

4. Simulation results and discussions

4.1. Thermo-fluid analysis

Fig. 2 shows the PEN temperature distributions in the MOLB-type SOFC under the first working conditions illustrated in Table 3. As comparing Fig. 2(a) with Fig. 2(b), two characteristic features can be seen. One is that the PEN average temperature is 1014 K with maximum and minimum temperatures of 1063

Table 3
The cell operating conditions and parameters used for simulation

Sample number	Fuel			Air		Flow pattern
	Delivery rate ($v1$) ($\mathrm{m\,s^{-1}}$)	Inlet temperature (K)	Hydrogen mass fraction (%)	Delivery rate ($v2$) ($\mathrm{m\,s^{-1}}$)	Inlet temperature (K)	
1	0.5	973	0.8	3	873	Counter-flow, Co-flow
2	0.5 1.0 1.5	973	0.8	3	873	Co-flow
3	0.5	973	0.8 0.9 1	3	873	Co-flow
4	0.5	973	0.8	3 2 1	873	Co-flow

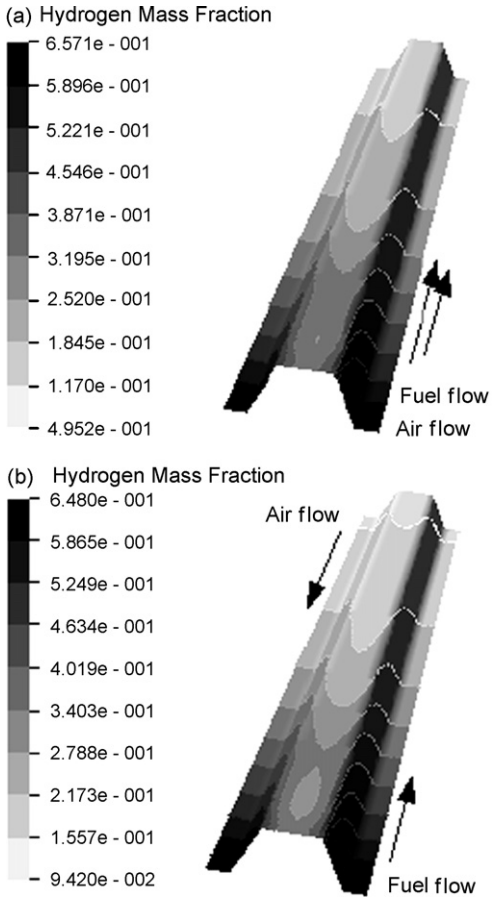

Fig. 3. Hydrogen mass fraction distributions on the interface between anode/electrolyte in the co-flow case (a) and counter-flow case (b) under first working conditions.

and 987 K in MOLB-type SOFC in co-flow case (see Fig. 2(a)). But, in counter-flow case, average temperature is 996 K with maximum and minimum temperatures of 1088 and 923 K (see Fig. 2(b)). So the co-flow case has the more uniform temperature distribution and smaller temperature difference (ΔT) from air inlet to outlet. A further difference is that the temperature of PEN increases uniformly along the direction of fuel flow, and is highest near the fuel outlet in co-flow case. However, the temperature of PEN rises rapidly, reaching a maximum near the fuel inlet, and then gradually drops for counter-flow case. This is due to the offsetting effects of air near the inlet, at its coolest, being aligned with the fuel inlet. As a consequence, the temperature gradient is smaller in co-flow case, which must result in the smaller thermal stress in the PEN although the thermal stress distributions were not researched in the paper.

Fig. 3(a and b) illustrates the hydrogen mass fraction distributions in the co-flow and counter-flow cases, respectively. Along the direction of fuel flow, the mass fractions of hydrogen on the interface between the electrolyte and anode decrease due to the electrochemical reaction. In particular, of the two flow case, the hydrogen mass fraction near the fuel outlet is less in co-flow case, so the more fuel is consumed and fuel utilization is higher accordingly.

On the basis of above analysis about the temperature distribution, it was found that the co-flow case is advantageous to improve the fuel utilization and mitigate the steep temperature gradient, and hence to reduce the internal stresses. For the co-flow case, other working conditions influenced the performances of SOFC were also studied. Firstly, we characterized the effects of the fuel gas on current density and temperature distributions. Fig. 4 shows the current density distributions of PEN. Changing the delivery rate of fuel with 0.5, 1.0 and 1.5 m s^{-1}, respectively, the average current density gradually increases (see Fig. 4(a–c)), but the current density is less uniform. This indicates that it is effective for the improvement of the electrical performance to increase the delivery rate of fuel. Fig. 5(a) shows the temperature distributions of the mid-plane in the X-direction. With the increment of the delivery rate of fuel, the average temperature and temperature difference (ΔT) from fuel inlet to outlet of PEN rise, so the temperature gradient also rises, which may cause thermal stress.

Then, we focus on the influence of hydrogen proportion in fuel on the temperature and current density distributions. Changing the hydrogen mass fraction in the fuel gas with 0.8, 0.9 and 1.0, reaction rate rise and more hydrogen is consumed, and then the more reaction heat is accumulated. As a result, the temperature gradient and current density also rise, as shown in Fig. 5(b) and Fig. 6(a–c). Furthermore, as comparing Fig. 4 with Fig. 6, with higher delivery rate of hydrogen, current density distributions were less uniform, but with larger mass fraction of hydrogen in fuel gas, current density distributions are more uniform.

In order to decrease the temperature gradient, it is effective to increase delivery rate of air. In the SOFC system, air not only provides oxygen ions but also has the cooling function.

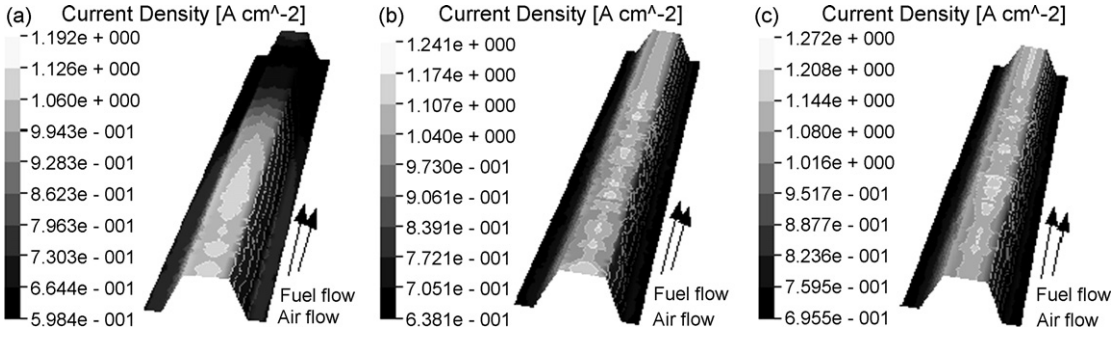

Fig. 4. Current density distributions on the interface of anode/electrolyte for the MOLB-type SOFC in the co-flow case under second working conditions.

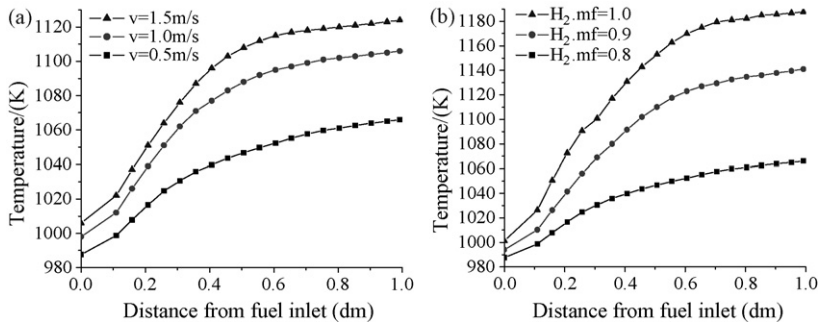

Fig. 5. PEN temperature distributions for MOLB-type SOFC under the second working conditions (a) and third working conditions (b).

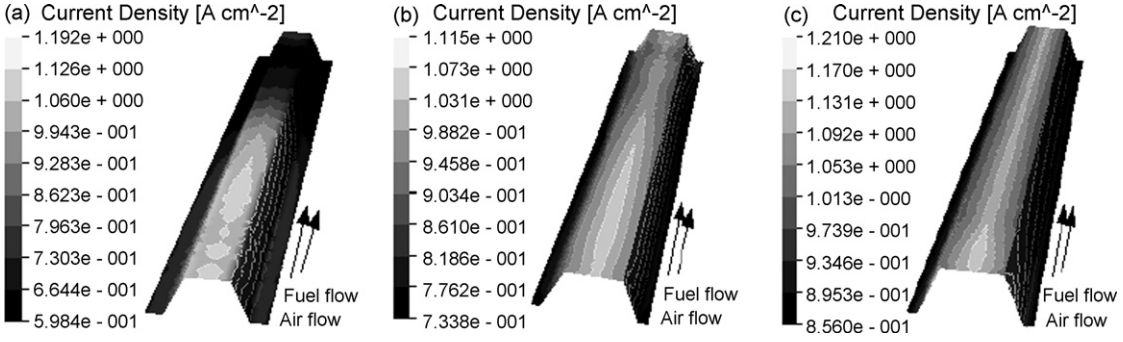

Fig. 6. Current density distributions on the interface of anode/electrolyte for MOLB-type SOFC under third working conditions.

Increasing the delivery rate of air, the steep temperature gradient is mitigated in MOLB-type SOFCs, as shown in Fig. 7. This is because more reaction heat is absorbed and then released by the air with the higher delivery rate, although the air utilization is dropped.

4.2. Advantage of MOLB-type SOFC compared with planar SOFC

On the basis of the preceding works about the simulating the planar SOFC system [26], the general trends of the temperature distributions in the planar and MOLB-type SOFCs are similar in essential. Although the average temperatures in MOLB-type SOFC are higher than those in the planar, the temperature difference (ΔT) is lower in MOLB-type SOFC. This is because the electrochemical reaction area of MOLB-type SOFC is larger and the more fuel is consumed in the active areas, as result, the more hydrogen is consumed and more reaction heat is accumulated. However, due to the effect of corner formed by the inclined plane and the upper plane, the temperature and hydrogen mass fraction distributions in MOLB-type SOFC are less uniform than those in the planar.

As comparing the current density distribution in planar SOFC with that in the MOLB-type SOFC, some main characteristic features can be seen. The first feature is that, in the two kinds of SOFCs, the current densities gradually decrease along the fuel flow direction because of the dropping of hydrogen mass fraction. And the second is that, average current densities are higher than those in the planar SOFC due to the larger reaction areas in MOLB-type one, but the current density distributions are less uniform in the MOLB-type SOFC. This is because, the current densities not only decrease along the fuel flow direction

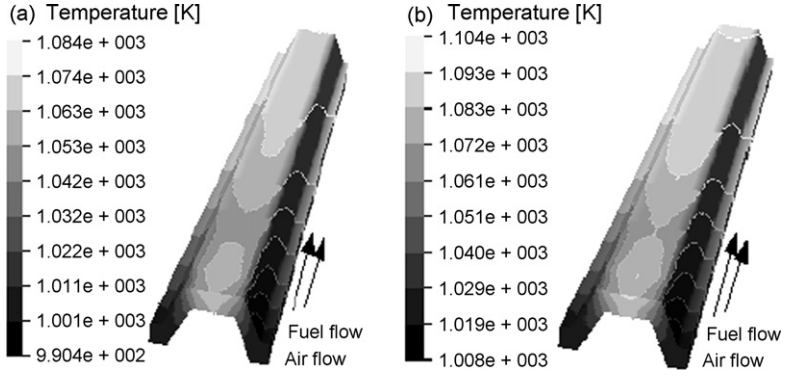

Fig. 7. PEN temperature distributions for MOLB-type SOFC under forth working conditions.

but also change along the incline plane and reach the maximum on the top plane due to the gathering current density function of the inter-connector. The last characteristic is that, with the increase in the delivery rate and mass fraction of hydrogen, the increment of the temperatures and current densities are less than those in planar SOFC.

5. Conclusions

The exchange current density was used to couple the thermo-fluid model with electrochemical model. The performances of MOLB-type SOFCs in stead state were calculated and compared with the performances of the planar SOFC. Some main conclusions were made as follows:

The PEN temperature distribution in the MOLB-type one is more uniform in co-flow case than that in counter-flow case, in particular, the temperature gradient is lower and current density is higher than those in the planar SOFC.

For co-flow case, with increasing the delivery rate of fuel gas or hydrogen mass fraction in the fuel, temperature gradients and average current densities rise in the MOLB-type SOFC. But increasing delivery rate of air, steep temperature gradients are mitigated. In particular, with the same increasing in delivery rate of fuel and hydrogen mass fraction, the increment of temperature distributions in MOLB-type SOFC are less. The current density distributions are less uniform with higher delivery rate of fuel, and are more uniform with larger mass fraction of hydrogen in fuel.

Acknowledgement

The authors gratefully acknowledge the contribution of the National Nature Science Foundation of China (NSFC Nos. 50675081 and 50475134).

References

[1] S.C. Singhal, Solid State Ionics 135 (2000) 305–313.
[2] S.C. Singhal, Solid State Ionics 152–153 (2002) 405–410.
[3] B. Godfrey, K. Foger, R. Gillespie, R. Bolden, S.P.S. Badwal, J. Power Sources 86 (2002) 68–73.
[4] G.Y. Xie, K. Cui, J.Z. Xiao, X.L. Qian, J. HuaZhong Univ. Sci. Tech. 30 (2002) 90–92 (in Chinese).
[5] H.W. Zheng, K.S. Ru, X.J. Zhang, J. Southwest China Normal Univ. 27 (2002) 789–793 (in Chinese).
[6] S.P. Simner, J.F. Bonnett, N.L. Canfield, K.D. Meinhardt, J.P. Shelton, V.L. Sprenkle, J.W. Stevenson, J. Power sources 113 (2003) 1–10.
[7] T. Fukui, S. Ohara, M. Naito, K. Nogi, J. Power Sources 110 (2002) 91–95.
[8] S.P. Jiang, Y.Y. Duan, J.G. Love, J. Electrochem. Soc. 149 (2002) A1175–A1183.
[9] V.V. Kharton, E.V. Tsipis, A.A. Yaremchenko, J.R. Frade, Solid State Ionics 166 (2004) 327–337.
[10] T. Ishihara, S. Fukui, H. Nishiguchi, Y. Takita, J. Electrochem. Soc. 149 (2002) A823–A828.
[11] T. Hibino, A. Hashimoto, M. Suzuki, M. Yano, S. Yoshida, M. Sanob, J. Electrochem. Soc. 149 (2002) A195–A200.
[12] Z. Lin, J.W. Stevenson, M.A. Khaleel, J. Power Sources 117 (2003) 92–97.
[13] J.J. Hwang, C.K. Chen, D.Y. Lai, J. Power Sources 140 (2005) 235–242.
[14] M. Iwata, T. Hikosaka, M. Morita, T. Iwanari, K. Ito, K. Onda, Y. Eaaki, Y. Sakaki, S. Nagata, Solid State Ionics 132 (2000) 297–308.
[15] H. Yakabe, T. Ogiwara, M. Hishunuma, I. Yasuda, J. Power Sources 102 (2001) 144–154.
[16] H. Yakabe, T. Sakurai, Solid State Ionics 174 (2004) 295–302.
[17] H. Yakabe, Y. Baba, T. Sakurai, M. Satoh, I. Hirosawa, Y. Yoda, J. Power Sources 131 (2004) 278–284.
[18] K.P. Recknagle, R.E. Williford, L.A. Chick, D.R. Rector, M.A. Khaleel, J.Power Sources 113 (2003) 109–114.
[19] N. Autissier, D. Larrain, J. Van herle, D. Favrat, J. Power Sources 131 (2004) 313–319.
[20] Y. Shiratori, Y. Yamazaki, J. Power Sources 114 (2003) 80–87.
[21] J.J. Hwang, J. Fuel Cell Sci. Technol. 2 (2005) 164–170.
[22] J.J. Hwang, C.K. Chen, D.Y. Lai, J. Power Sources 143 (2005) 75–83.
[23] S.G. Neophytides, Chem. Eng. Sci. 54 (1999) 4603–4613.
[24] M. Iwata, T. Hikosaka, M. Morita, T. Iwanari, K. Ito, K. Onda, Y. Esaki, Y. Sakaki, S. Nagata, Solid State Ionics 132 (2000) 297–308.
[25] G.-T. Tang, Z.-Y. Luo, M.-J. Ni, C.-J. Yu, K.-F. Chen, Preceeding of CSEE 25 (2005) 116–121 (in Chinese).
[26] G. Wang, Y. Yang, H. Zhang, W. Xia, J. Power Sources 167 (2006) 398–405.
[27] J. Huang, Numerical Simulation of Heat and Mass Transfer in Solid Oxide Fuel Cell, Nanjing University of Science &Technology, 2004 (in Chinese).
[28] H. Yang, W. Lu, Applied electrochemical, Scientific Publishing Center, Beijing, PR China, 2001 (in Chinese).
[29] S.H. Chan, K.A. Khor, Z.T. Xia, J. Power Sources 93 (2001) 130–140.